Impact of CO_2 geological sequestration on the nucleation of earthquakes

Frédéric Cappa[1,2], and Jonny Rutqvist[1]

[1] *Lawrence Berkeley National Laboratory, Earth Sciences Division, University of California, Berkeley, USA*

[2] *GeoAzur, University of Nice Sophia-Antipolis, Côte d'Azur Observatory, France*

E-mail addresses: cappa@geoazur.unice.fr (F. Cappa); jrutqvist@lbl.gov (J. Rutqvist)

ABSTRACT

[1] *Can CO_2 storage cause earthquakes? What is the maximum possible earthquake magnitude resulting from CO_2 injection?* Here, as a theoretical case study we investigate these questions using coupled hydromechanical modeling with multiphase flow and seismological variables for quantifying earthquake magnitude and energy. Our simulations consider transient fluid flow and stress coupling, and the evolution of fault properties. We simulate CO_2 injection into a reservoir-caprock system bounded by a subvertical normal fault subjected to different extensional stress regimes and over a range of initial fault permeability values. For our assumed system and injection rate, the simulation results show that sudden stress drop and fault slip primarily initiated along the fault portion intersecting the storage reservoir after a few months of injection when a sufficiently high reservoir pressure has been reached. The size of the rupture area, and consequently, the earthquake magnitude and energy, depends on initial horizontal-to-vertical stress ratio and fault permeability, which strongly influences the size of the pressurized area, and subsequent stress variations.

1. Introduction

[2] In some geological settings, fluid injection in underground reservoirs is known to trigger earthquakes, though mostly of smaller magnitudes ($-3 < M_w < 2$). Occasionally, however, earthquakes with larger magnitudes occur ($2 < M_w < 5$) [*Shapiro and Dinske*, 2009]. Several lines of evidence indicate that parts of the Earth's crust are close failure, and small perturbations of the fluid pressure and stress can lead to seismic events [*Zoback and Harjes*, 1997]. Fluid-injection-induced seismicity has been extensively studied in the context of geothermal systems; and it has been shown that the hydromechanical interactions can be strongly nonlinear, involving rock hydraulic diffusivity, elastic properties and rupture. In this paper, we investigate the impact of a local CO_2 injection in a deep underground reservoir on the nucleation of seismic fault ruptures. We address the following two questions: (1) Can CO_2 storage cause sudden fault slip and earthquakes? (2) What is the maximum possible earthquake magnitude resulting from CO_2 injection in a faulted reservoir?

[3] This study builds on a previous study [*Cappa and Rutqvist*, 2011] in which we considered the CO_2-injection-induced aseismic rupture along a fault zone with constant friction, neglecting frictional weakening during plasticity. In Cappa and Rutqvist [*2011*] we compared different fault mechanical behavior and presented several key results, including that the most simple mechanical approach, isotropic Mohr-Coulomb type plasticity, is adequate for modeling coupled hydromechanical processes during fault reactivation. We also showed that shear-enhanced fault permeability plays an important role in propagating fault instability and permeability enhancement through the overlying caprock. Here, noting that a substantial drop in friction may occur during seismic fault-rupture nucleation and propagation, we extend this previous work to include frictional weakening. We consider in this study the widely used slip-weakening friction model, although the rate and state friction law describes the whole friction evolution, with friction increasing with slip velocity before falling to low dynamic levels [*Marone et al.*, 2009]. We present results for a case in which a normal fault bounds a storage reservoir between two caprocks. This representation corresponds to a critical geometrical case for fault reactivation during a CO_2 injection [*Hawkes et al*., 2004]. We first present a general review of the seismological variables involved in related fault-instability processes. Thereafter, we examine how CO_2 injection affects the distribution and magnitude of fault slip and, consequently, the

ruptured zone. Based on comparison of our numerical simulations, we show that for broad ranges of realistic parameters, the rupture dimension and slip magnitude are sensitive to permeability as well as to the ratio between the initial horizontal and vertical stress. The simulations were performed using the coupled thermo-hydro-mechanical simulator TOUGH-FLAC, which is described in Rutqvist et al. [*2002*], and previously applied to study fault instability processes related to multiphase fluid flow and crustal deformations [*Rutqvist et al*., 2007; *Cappa et al*., 2009; *Cappa and Rutqvist*, 2011]. Finally, from the model simulation results we estimate the possible earthquake magnitudes induced for our CO_2 injection scenario, and provide a comparison with seismological data of natural and induced earthquakes from other studies.

2. Seismological variables used to quantify earthquake properties

[4] Several seismological studies indicate that an earthquake can be viewed as a stress-release process on a surface of area (A) [*Kanamori and Brodsky*, 2004]. In the simplest case, fault-weakening behavior occurs during rupture propagation, generally represented by the shear stress (τ) evolution as a function of slip (d), and called the "slip-weakening model" [*Kanamori and Brodsky*, 2004]. The main parameters describing the slip-weakening model are the initial yield and residual shear stresses and the critical slip (d_c) over which the fault linearly weakens. At the start of an earthquake, the resisting stress on the fault plane drops from the initial shear stress (τ_0) to a final stress (τ_f). The difference between initial and final stresses is the static stress drop ($\Delta\sigma_s = \tau_0 - \tau_f$). Despite fault-weakening representing most of the shear stress evolution, slip hardening can often precede the beginning of the breakdown phase. Laboratory experiments suggest that d_c is typically tens of microns at low slip velocity and several meters at high slip velocity, whereas seismological observations suggest that d_c can range from 0.05 to 1 m [*Tinti et al*., 2009]. Several studies also found that d_c is generally proportional to the final slip, with d_c ranging from 20 to 90% of d.

[5] With seismological methods, one can determine d, A and the slip velocity (V_D). Given the shear modulus of crustal rocks (μ), and the shear-wave velocity (V_S), the dynamic and static stress drops are calculated as $\Delta\sigma_d = \mu V_D/V_S$, and $\Delta\sigma_s = \mu d/A^{1/2}$. Both stress drops typically range from 0.1 to 100 MPa for moderate and large earthquakes [*Scholz*, 2002; *Griffith et al.*, 2009]. The static stress drop can also be estimated from $\Delta\sigma_s = (7M_0/16r^3)$ [*Eshelby*, 1957], where M_0 is the seismic

moment and *r* the radius of a circular fault.

[6] The quantification of the overall size of an earthquake is generally based on the seismic moment defined by $M_0 = \mu A d$. Most data compilations find that seismic moment and ruptured fault area are related as $M_0 \propto A^{3/2}$, because, at least for a circular rupture, M_0 varies as $M_0 \propto \Delta\sigma_s A^{3/2}$ [*Aki*, 1967]. Then the magnitude (M) of an earthquake is given, in terms of seismic moment, by $M = (\log_{10} M_0 / 1.5) - 10.73$ [*Kanomori and Anderson*, 1975].

3. Numerical model and conditions

[7] Fig. 1a shows the geometry and initial conditions of the basic model, which is discretized into a two-dimensional plane strain model (2 km × 2 km). The model extends vertically from 500 m to 2500 m in depth and horizontally far enough from the injection zone (2 km) to simulate laterally infinite acting conditions. The horizontal size of the model was chosen from a sensitivity study indicating that this size does not affect results in the zone of interest. The model consists of a storage aquifer 100 m in thickness, bounded at the top and bottom by a low-permeability 150 m thick caprock, which, in turn, is surrounded by two other aquifers extending vertically 1650 m below and 1350 m above, respectively. This multilayer system is intersected by a pre-existing normal fault with a dip angle of 80°, width of 2.5 m, and length of 2 km. The fault and the injection point are spaced 500 m apart horizontally. In this case, we envision a fault with an offset of 125 m, so that the offset will laterally limit the reservoir.

[8] In the simulations, CO_2 is injected as a point source at 1500 m depth with a constant rate of 0.02 kg/m/s (i.e. 630.72 tons/m/year) (Fig. 1a). At this depth, initial fluid pressure and temperature (P = 14.72 MPa and T = 47.5 °C) assure supercritical conditions for CO_2. The temperature is assumed to be 22.5°C at 500 m depth and 72.5°C at 2500 m depth, resulting in a depth gradient of 25°C/km and assuming a temperature of 10°C on the ground surface. The initial fluid pressure at 500 m depth is 5 MPa and 24.63 MPa at 2500 m, considering a hydrostatic gradient (9.81 MPa/km) and atmospheric pressure of 0.1 MPa at the ground surface. Constant pressure, saturation, and temperature conditions are assumed at the boundaries, except for the left boundary, where no flow occurs. That is, the other boundaries are open for fluid flow. Simulations are conducted in an isothermal mode, which implies that the thermal gradient is

maintained according to the initial conditions. Null displacement conditions were set normal to the left and bottom boundaries, whereas stress was set to the right and top boundaries. An extensional stress regime ($\sigma_h = 0.7\sigma_v$, considering a vertical stress gradient of 2.217×10^4 MPa/m, and a bulk density of 2260 kg/m^3) was assumed.

[9] To provide a context for the parametric study presented in the Section 4.2, we first discuss results for multiphase fluid flow and ruptures for a reference case whose hydraulic and mechanical properties are given in Table 1. Properties for the permeable aquifers and the caprocks represent sandstone and shale, respectively. Reservoir rocks are considered to be elastic, whereas elasto-plastic behavior is considered for the fault, including an anisotropic Mohr-Coulomb model (ubiquitous joints presented in Cappa and Rutqvist [*2011*]) obeying frictional weakening from a static friction coefficient of 0.6 to a residual value of 0.2 over a critical plastic strain of 1×10^{-3} (Fig. 1b), consistent with the slip-weakening model commonly used in seismology to simulate earthquake rupture dynamics [*Templeton and Rice*, 2008]. We use a permeability model in which permeability changes with volumetric strain and porosity according to Rutqvist and Cappa [*2011*], while we use a zero dilation angle for the fault. This implies that permeability can change as a result of changes in effective stress and volumetric strain, but there is no shear-induced permeability change along the fault. Instead we consider the effect of different fault permeability in a sensitivity study.

[10] The fluid-property module ECO2N [*Pruess and Spycher*, 2007] was employed for modeling the thermodynamic and thermophysical properties of water-NaCl-CO_2 mixtures. The relative permeability of gas and liquid phases is calculated from Corey's function [*Corey*, 1954], while capillary pressure is governed by the van Genuchten's function [*van Genutchen*, 1980].

4. Modeling results

4.1 Reference case

[11] Modeling results for the reference case are illustrated in Figs. 1c to f, and show that a sudden fault slip occurs after 90 days of CO_2 injection (Fig. 1c). This slip event is instantaneous and can radiate seismic waves. The slip then propagates aseismically. In the fault portion intersecting the reservoir, the slip magnitude ranges between 1 and 7 cm from the upper to the bottom limit of the

reservoir. Figs. 1d-e indicate that the fluid pressure buildup is mainly located in the reservoir, at the contact with caprocks and the fault, whereas the CO_2 is mainly situated near the injection point. Fluid pressurization (~ 10 MPa) induces intense plastic shear strain distributed over a length of about 385 m with a maximum value of 1×10^{-2}, in a portion of the fault just below the reservoir (red zone in Fig. 1f). The ruptured zone affects both the fault portion inside the reservoir where the fluid pressure increases, as well as a large portion of the fault below the reservoir, where stresses increase due to the forcing imposed by the expanding reservoir. Fig. S1 of the auxiliary material shows that the fluid-pressure increase produces a progressive increase in shear stress and a slow decrease in shear strength along the fault over the first 90 days of CO_2 injection. Then at a critical state, a sudden reduction in shear strength triggers shear slip. During the slip event, the friction decreases over a critical slip distance to the residual value as a result of the generation of plastic shear strain along the fault. Fig. 2 illustrates the changes in fluid pressure, stress, slip and permeability along the fault during the abrupt slip. In the model, we considered that these changes correspond to the co-seismic phase of an earthquake. The profiles show that the fluid-pressure increases of 0.2 MPa along the fault portion in the reservoir accompanied a decrease in effective stress of 0.2 MPa. Over the ruptured zone, the maximum shear stress drop is 2 MPa, and the maximum slip is 8 cm. The slip event produces a small increase in fault permeability, mainly localized within the portion intersecting the reservoir. This fault permeability change is mainly caused by reduction in effective stress in the zone of significant increase in fluid pressure. The calculated slip and stress-drop magnitudes turn out to be reasonable when compared to data from others studies of natural earthquakes [*Scholz,* 2002].

[12] From these simulation results and the relationships presented in Section 2, we can calculate the seismic moment from the mean slip over the ruptured area, the rock shear modulus ($M_0 = \mu A d$), and the radiated energy from the static stress drop ($E_R \approx (\Delta\sigma_s/2\mu)\cdot M_0$). Since our simulations are conducted in a plane strain model, we can assume a unit lateral extent for rupture (i.e., L = 1 km). Thus, a seismic moment of $M_0 = 4 \times 10^9 \times 1000 \times 385 \times 0.08 = 1.23 \times 10^{14}$ Nm, and a radiated energy of $E_R = [0.42 \times 10^6 / (2 \times 4 \times 10^9)]/ 1.23 \times 10^{14} = 6.46 \times 10^9$ J are estimated for the slip event induced by the CO_2 injection simulated here, at 500 m from the causative fault (Fig. S2 of the auxiliary material).

[13] In summary, our simulations show typical fault behavior with a slow accumulation of elastic stresses and strain along a locked fault, until a sudden rupture with associated increase in seismic moment and radiated energy (Fig. S2 of the auxiliary material).

4.2 Sensitivity analysis

[14] We examined the sensitivity of the slip magnitude and length to the initial fault permeability and stress ratio (σ_h/σ_v). Results are illustrated in the phase diagrams presented in Fig. 3. Our parametric analysis shows that fault slip and rupture width are mainly sensitive to the stress ratio and less significantly affected by the fault permeability. The most substantial slip is found for the highest stress ratio ($\sigma_h = 0.6\sigma_v$) with a magnitude greater than 0.7 m along a fault entirely ruptured. However, for this high stress ratio, the size of the model (2 km) is certainly too small, and consequently, fault slip is influenced by the model boundaries.

[15] In summary, our parametric analysis indicates that the higher the stress ratio, the higher the slip, and the larger the rupture length. In addition, the rupture initiation is reached earlier when the stress ratio is high, because the state-of-stress is near the frictional strength limit; consequently, very small stress perturbations may facilitate triggering of earthquakes. In addition, a fault with low permeability will accelerate the initiation of slip, because fluid pressure buildup sufficient for failure is reached faster than in a high permeability fault, in which fluid tends to diffuse more readily.

4.3 Estimation of the seismic moment and magnitude

[16] Our simulations indicated possible earthquake magnitudes ranging from 1.4 to 4.5 for different extensional stress regimes (Table 2) applied to a normal fault optimally oriented for seismic slip. This estimation of magnitude agrees with the earthquake scaling obtained by [*Viegas et al*., 2010] from the compilation of seismic moment versus source radius, for a large population of natural and induced earthquakes reported in other studies (Fig. 4).

5. Discussion and conclusion

[17] Large-scale storage of CO_2 in deep underground reservoirs may cause considerable pore-pressure perturbation as well as flux migration; and, concern has been raised over whether nearby

faults could be reactivated. Here, we simulated a local CO_2 injection into a reservoir-caprock system bounded by a subvertical normal fault with different extensional stress regimes and permeability. This configuration represents a critical geometrical case, because the injection-induced fluid-pressure increase penetrates the fault plane and strongly increases the risk of fault reactivation. We utilized a frictional-weakening model to simulate the possibility of seismic slip, as highlighted in seismological studies. Our results showed that a sudden stress drop (up to a few MPa) and fault slip (up to tens of centimeters) primarily occur along the fault portion intersecting the storage reservoir after a few months of injection. Some portions of the fault outside the storage reservoir also fail in response to fluid and stress transfer from the pressurized fault portions. At high stress ratios, typically 0.6 in our study, the fault is entirely ruptured over the vertical extent of our model, but for lower stress ratio ($\sigma_h/\sigma_v > 0.6$), the fault is not entirely reactivated seismically. The size of the rupture area, and consequently the earthquake magnitude and energy, is also related to fault permeability, which strongly influences the size of the pressurized area, and subsequent stress variations. At high stress ratios, the maximum earthquake magnitude is estimated to 4.5.

[18] Our analysis provides important results for understanding faulting in reservoirs, and for seismic-potential assessment of areas involved in CO_2 sequestration. Further studies coupling a hydromechanical analysis with seismic waves radiated by fault slip events is a high priority for better understanding earthquake ruptures and the associated damage of the reservoir-caprock system during CO_2 storage. It is important to clarify such effects and to test the rupture predictions with field observations, because earthquake faults can allow gas to escape towards the ground surface. Finally, we should clarify that our simulations were conducted to intentionally induce fault reactivation, which occurred a high reservoir pressure in an unfavourable stress regime. In a future commercial scale CO_2 operation, the injection pressure should be carefully controlled and monitored to avoid fault reactivation. The admissible injection pressure at a particular site will be strongly dependent on the in situ stress field as shown in this study.

Acknowledgements

[19] The work presented in this paper was financed by the Assistant Secretary for Fossil Energy, Office of Natural Gas and Petroleum Technology, through the National Energy Technology

Laboratory, under the U.S. Department of Energy Contract No. DE-AC02-05CH11231. We thank Gisela Viegas at the Lawrence Berkeley National Laboratory for providing us the earthquake data and MATLAB routines to generate the Fig. 4. We thank Dan Faulkner for his constructive review and suggestions that improved our paper.

References

Aki, K. (1967). Scaling law of seismic spectrum, *J. Geophys. Res.*, 72(4), 1217-1231.

Cappa, F., Rutqvist, J., and Yamamoto, K. (2009). Modeling crustal deformation and rupture processes related to upwelling of deep CO_2-rich fluids during the 1965–1967 Matsushiro earthquake swarm in Japan, *J. Geophys. Res.*, 114, B10304, doi:10.1029/2009JB006398.

Cappa F., and Rutqvist J. (2011). Modeling of coupled deformation and permeability evolution during fault reactivation induced by deep underground injection of CO_2. *Int J Greenhouse Gas Control*, 5, 336-346, doi:10.1016/j.ijggc.2010.08.005

Corey A.T. (1954). The interrelation between oil and gas relative permeabilities, Producers Monthly, 38-41.

Eshelby, J.D. (1957), The determination of the elastic field of an ellipsoidal inclusion and related problems, *Proc. R. Soc. London*, 241, 376-396.

Griffith, W.A., Di Toro, G., Pennacchioni, G., Pollard, D.D., and Nielsen, S. (2009). Static stress drop associated with brittle slip events on exhumed faults, *J. Geophys. Res.*, 114, B02402, doi:10.1029/2008JB005879.

Hawkes, C.D., McLellan, P.J., Zimmer, U., and Bachu, S. (2004). Geomechanical factors affecting geological storage of CO2 in depleted oil and gas reservoirs: risks and mechanisms. In: *Proceedings of Gulf Rocks 2004, the 6th North America Rock Mechanics Symposium (NARMS): Rock Mechanics Across Borders and Disciplines*, Houston, Texas.

Kanamori, H., and Anderson, D.L. (1975). Theoretical basis of some empirical relations in seismology, *Bull. Seism. Soc. Am.*, 65, 1073-1095.

Kanamori, H., and Brodsky, E.E. (2004). The physics of earthquakes, *Reports on Progress in Physics*, 67(8), 1429-1496.

Marone, C., Cocco, M., Richardson, E., Tinti, E. (2009). The critical slip distance for seismic and aseismic fault zones of finite width, *In: Fault-zone Properties and Earthquake Rupture Dynamics, edited by E. Fukuyama, International Geophysics Series*, 94, 135-162, Elsevier.

Pruess, K., and Spycher, N. (2007). ECO2N – A fluid property module for the TOUGH2 code for studies of CO2 storage in saline aquifers, Energ. Conv. Man., doi:10.1016/j.enconman.2007.01.016.

Rutqvist, J., Wu, Y-S., Tsang, C-F., and Bodvarsson, G. (2002). A modeling approach for analysis of coupled multiphase fluid flow, heat transfer, and deformation in fractured porous rock, *Int J Rock Mech Min Sci*, 39:429-442.

Rutqvist J., Birkholzer J.T., Cappa F., and Tsang C-F. (2007). Estimating maximum sustainable injection pressure during geological sequestration of CO_2 using coupled fluid flow and geomechanical fault-slip analysis. *Energy Conv Man*, 47:1798-1807.

Scholz, C. H. (2002). The mechanics of earthquakes and faulting, *2nd ed. Cambridge University Press*, Cambridge, 471 pp.

Shapiro, S.A., and Dinske C. (2009). Scaling of seismicity induced by nonlinear fluid-rock interaction, *J. Geophys. Res.*,114, B09307, doi:10.1029/2008JB006145.

Templeton, E.L., and Rice J.R. (2008). Off-fault plasticity and earthquake rupture dynamics: 1. Dry materials or neglect of fluid pressure changes, *J. Geophys. Res.*, **13**(B9), B09306.

Tinti, E., Cocco, M., Fukuyama, E., and Piatanesi, A. (2009). Dependence of slip weakening distance (D_c) on final slip during dynamic rupture of earthquakes, *Geophys. J. Int.*, 177, 1205-1220, doi :10.1111/j.1365-246X.2009.04143.x

van Genuchten, M.T. (1980). A closed-form equation for predicting the hydraulic conductivity of unsaturated soils, Soil. Sci. Soc. Am. J., 44:892-898.

Viegas, G., Abercrombie, R. E., and Kim, W-Y. (2010). The 2002 M5 Au Sable Forks, NY, earthquake sequence: Source scaling relationships and energy budget, *J. Geophys. Res.*, 115, B07310, doi:10.1029/2009JB006799.

Zoback, M., and Harjes, H.P. (1997). Injection-induced earthquakes and crustal stress at 9 km depth at the KTB deep drilling site, Germany, *J. Geophys. Res.*, 102, 18477-18491.

Table 1. Material properties used in the reference case, in which we assumed a stress ratio of $\sigma_h/\sigma_v = 0.7$.

Parameters	Storage Aquifer	Caprock	Others aquifers	Fault
Young's modulus	10 GPa	10 GPa	10 GPa	5 GPa
Poisson' ratio	0.25	0.25	0.25	0.25
Friction coefficient	-	-	-	0.2 to 0.6
Porosity	0.1	0.01	0.1	0.1
Permeability	10^{-13} m^2	10^{-19} m^2	10^{-14} m^2	10^{-16} m^2

Table 2. Estimated seismic moment (M_0) and magnitude (M_w) from mean slip (d_m), mean stress drop ($\Delta\sigma_m$) and rupture width (W) calculated in simulations for different ranges of stress ratio.

σ_H/σ_V	d_m (m)	$\Delta\sigma_m$ (MPa)	W (m)	M_0 (N.m)	M_w
0.6	0.85	1.1	2000	6.8×10^{15}	4.5
0.7	0.08	0.42	385	1.23×10^{14}	3.4
0.8	0.001	0.3	37.5	1.5×10^{11}	1.4

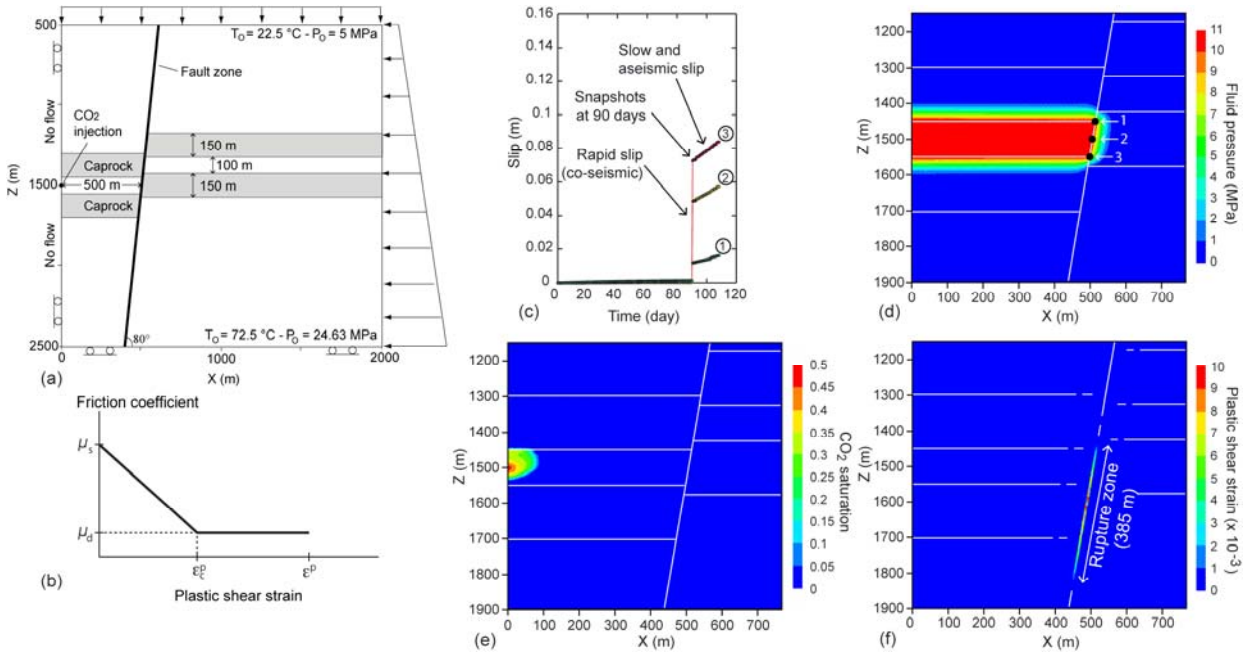

Figure 1. (a) Numerical model geometry and initial conditions. We assumed a normal fault with a 125 m offset through a 100 m thick reservoir bounded at the top and the bottom by a 150 m thick caprock. (b) A plastic shear strain-weakening friction law that governs the propagation of rupture along the fault zone. (c) Fault slip versus time at three points located at the (1) top, (2) middle and (3) bottom of the reservoir, respectively (see Figure 1d for the location). Snapshots of change (relative to the initial state) in (d) fluid pressure, (e) CO_2 saturation, and (f) plastic shear strain at the end of the sudden slip event (after 90 days of CO_2 injection).

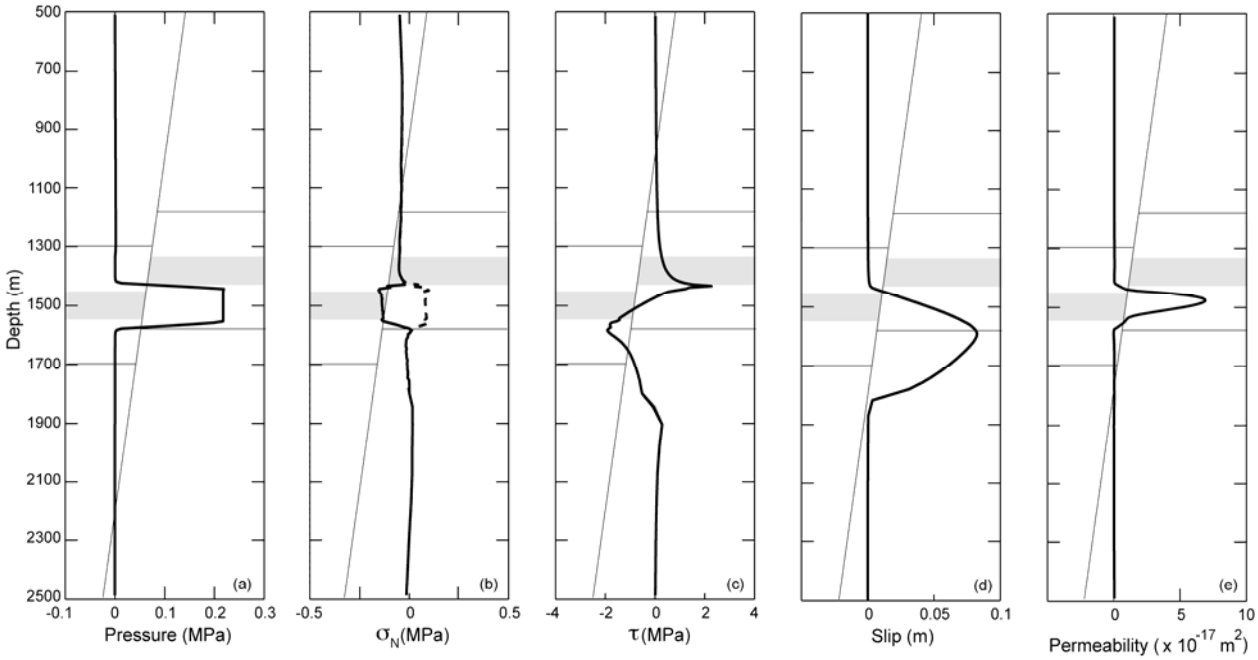

Figure 2. Vertical profiles of change in (a) fluid pressure, (b) total (dashed line) and effective (solid line) normal stress, (c) shear stress, (d) slip, and (e) permeability along the fault for the slip event (co-seismic phase).

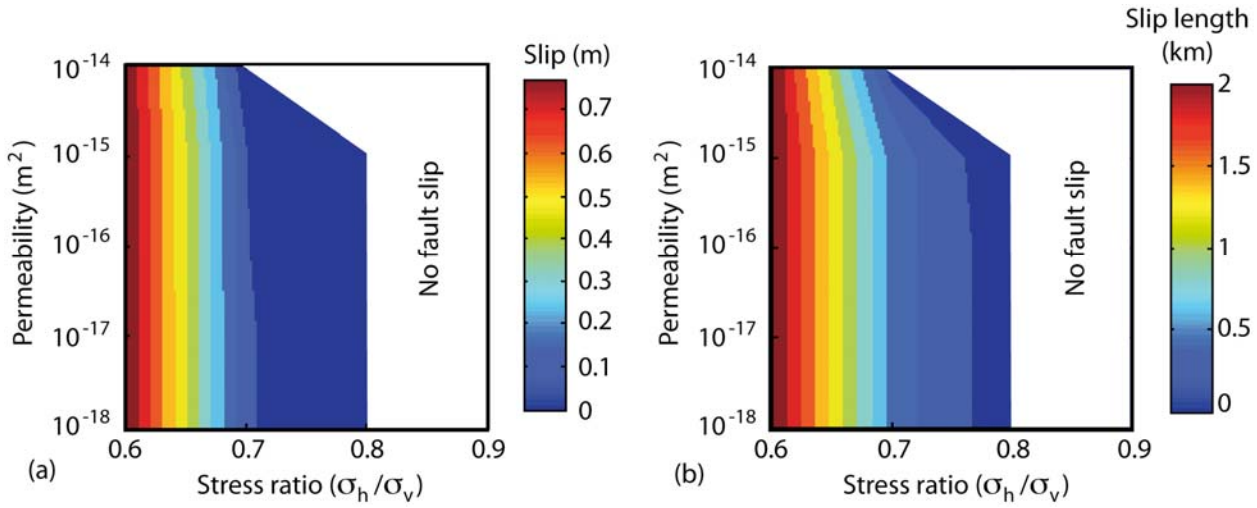

Figure 3. Phase diagrams illustrating the effects of the initial stress ratio (σ_h/σ_v) and permeability on the slip (a) magnitude, and (b) length.

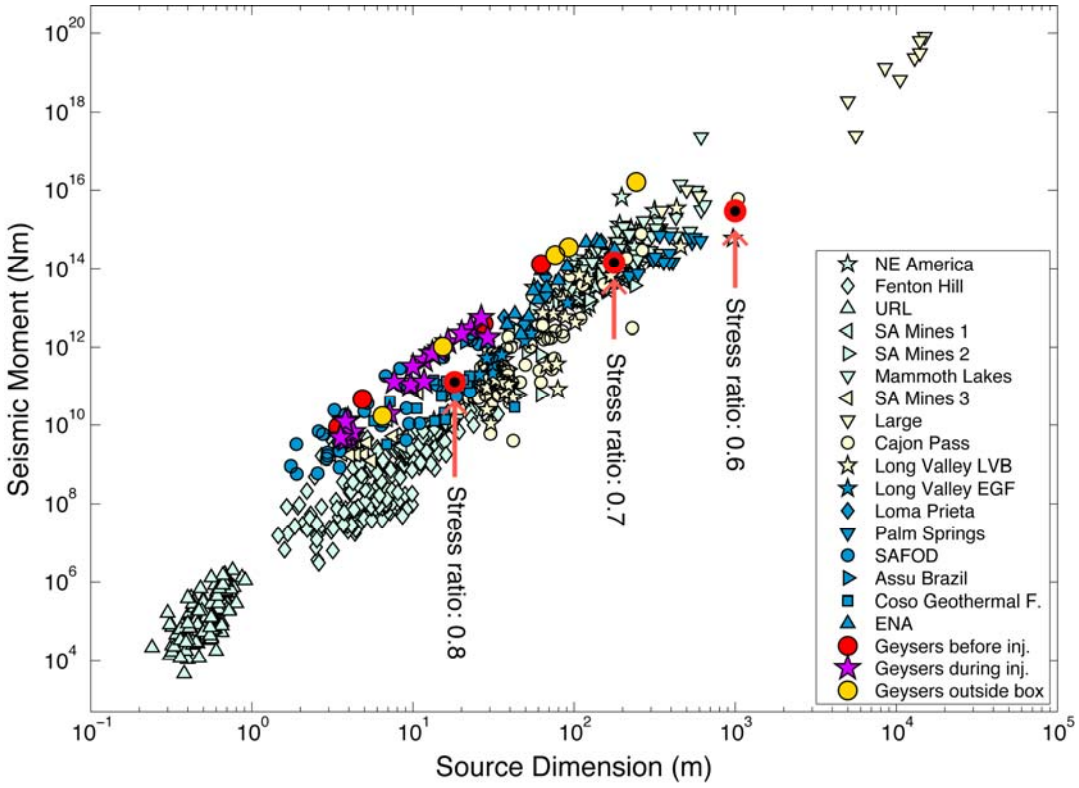

Figure 4. Earthquake scaling relationship after [*Viegas et al*., 2010]: source dimension (radius) and seismic moment. Red and black circles correspond to our simulation results for the stress ratio illustrated in Table 2.